Remote Sensing of Environment 271 (2022) 112923

Contents lists available at ScienceDirect

Remote Sensing of Environment

journal homepage: www.elsevier.com/locate/rse

Applications of a thermal-based two-source energy balance model coupled to surface soil moisture

Lisheng Song [a,b,*], Zhonghao Ding [b], William P. Kustas [c], Yanhao Xu [b], Gengle Zhao [b], Shaomin Liu [d], Mingguo Ma [b], Kejia Xue [b], Yan Bai [e], Ziwei Xu [d]

[a] School of Geography and Tourism, Anhui Normal University, China
[b] Chongqing Jinfo Mountain Karst Ecosystem National Observation and Research Station, School of Geographical Sciences, Southwest University, Chongqing 400715, China
[c] USDA, Agricultural Research Service, Beltsville Agricultural Research Center, Hydrology and Remote Sensing Lab, 10300 Baltimore Ave. BARC-West, Bldg. 007, Beltsville, MD 21738, USA
[d] State Key Laboratory of Earth Surface Processes and Resource Ecology, Faculty of Geographical Sciences, Beijing Normal University, Beijing 100875, China
[e] College of Atmospheric Sciences, Lanzhou University, Lanzhou 730000, China

ARTICLE INFO

Editor: Jing M. Chen

Keywords:
TSEB-SM model
Soil water stress
Surface flux estimation

ABSTRACT

The two-source energy balance (TSEB) model using the land surface temperature (LST) as a key boundary has been used to estimate land surface evapotranspiration (ET) over various landcovers and environmental conditions. However, LST may not always provide an adequate boundary condition to simultaneously constrain the soil evaporation and plant transpiration especially under water limited conditions. A refinement to TSEB model by coupling surface soil moisture information to derive the soil and vegetation component temperatures and a new transpiration algorithm was developed (TSEB-SM). The TSEB-SM model was evaluated under a wide range of surface soil water content values and vegetation cover conditions and compared with the performance with the original TSEB model using only LST. While the results showed that the TSEB-SM model produced similar agreement in the fluxes and ET as the original TSEB for the cropland and grassland sites, TSEB-SM model performance was notably improved at the shrub-forest and desert steppe sites with a significant reduction in mean absolute percent difference in daily ET from nearly 65% to 25% and from approximately 50% to 40%, respectively. It also appears to be more reliable in partitioning ET into soil evaporation and plant transpiration when compared to the partitioning using the water use efficiency (*uWUE*) approach in combination with the eddy covariance measurements. With satellite data such as MODIS LST and leaf area index, and surface soil moisture retrievals from microwave satellite observations, the TSEB-SM model may potentially be a more reliable tool for monitoring regional ET partitioning under sparse canopy cover conditions.

1. Introduction

Land surface evapotranspiration (ET) and its components of soil evaporation (E) and plant transpiration (T) are a nexus of the water, energy and carbon cycles (Jung et al., 2010), which has been applied in climate, hydrology, drought monitoring and crop yield predicting (Wang and Dickinson, 2012). The ET and *E* and *T* partitioning can be measured at canopy and patch scale representative areas, but it is very difficult to extrapolate these measurements to field, landscape and regional scales. Energy balance models using the land surface temperature (LST) as a key boundary condition have been applied to estimate convective and radiative exchange across the land-atmosphere interface. LST can be derived from ground measurements and observations from unmanned aerial vehicle (UAV), manned aircraft and satellite. These sources of LST observations have been used to primarily estimate ET from canopy to regional and global scales. The two-source energy balance (TSEB) model proposed by Norman et al. (1995) has been shown to address key convective and radiative exchange processes for many complex canopies, additionally partitioning the ET in to *E* and *T*. In the TSEB model, the plant transpiration was initially formulated using the Priestly-Taylor approach but other methods have been proposed such as the Penman-Monteith (TSEB-PM, Colaizzi et al. (2012)) or light use of

* Corresponding author at: School of Geography and Tourism, Anhui Normal University; Chongqing Jinfo Mountain Karst Ecosystem National Observation and Research Station, School of Geographical Sciences, Southwest University, China.
E-mail address: songls@ahnu.edu.cn (L. Song).

https://doi.org/10.1016/j.rse.2022.112923
Received 29 April 2021; Received in revised form 14 January 2022; Accepted 24 January 2022
Available online 3 February 2022

efficiency (TSEB-LUE, Anderson et al. (2008) and Houborg et al. (2011)), for more reliable estimation of the plant transpiration and introducing microwave soil moisture data to estimate the soil evaporation ($TSEB_{SM}$, (Kustas et al., 2003a, 2018).

In the original TSEB model, the value of Priestley-Taylor coefficient α_{PT} is initially assumed to equal its classic value of 1.26, and the value would decline as the canopy became water stressed which would be indicated by a modeled derived elevated soil temperature resulting in a negative daytime soil latent heat flux or condensation due to soil sensible heat flux exceeding the soil surface available energy, which is a non-physical solution during daytime convective conditions. This reduction in α_{PT} elevates the canopy temperature and modulates the derived soil temperature so that the value of daytime soil evaporation/latent heat flux will become greater than zero. However, under advective conditions where energy is being added beyond the available energy (net radiation less soil heat flux) the TSEB model is unable to account through any iterative solution for this additional evaporative demand but is shown to be related to the vapor pressure deficit (Agam et al., 2012). This can result in an underestimation of T and ET being underestimated under such advective conditions (Song et al., 2016). There may be other uncertainties in the model key boundary conditions, namely LST, leaf area index and green vegetation fraction (Kustas et al., 2019). The soil and canopy water use not only affects their kinetic temperatures which are estimated via the radiometric temperature observation, the key boundary of the TSEB model, and both temperatures are correlated to atmospheric demand and the soil moisture content affecting the evaporation from the soil surface and transpiration from plant stomata (Ait Hssaine et al., 2018; Gan and Gao, 2015; Kustas et al., 2003a, 2003b; Stocker et al., 2019). Remotely-sensed soil moisture information has been introduced into ET models providing additional constraints on soil evaporation improving performance of ET models such as Penman-Monteith and Priestley-Taylor mainly over the semi-arid regions (Brust et al., 2021; Purdy et al., 2018; Yao et al., 2017). The soil moisture constraint on plant transpiration should also be considered due to the land surface ET is often dominated by plant transpiration. Therefore, introducing information about the soil moisture content coupled to the transpiration algorithm in combination with the LST may be able to better constrain the transpiration estimates in the TSEB model, and as a result also improve the agreement with measured surface fluxes (Ait Hssaine et al., 2018; Song et al., 2016). In fact, Ait Hssaine et al. (2021) found that incorporating surface soil moisture from Sentinel-1 radar in the TSEB model significantly improved flux estimates over three semi-arid agricultural sites, mainly by adjusting the Priestley-Taylor coefficient α_{PT}.

In this study, the objective is (i) to define stress indices for constraining evaporation from soil surface and transpiration from the canopy, (ii) revise the TSEB model by introducing the surface soil moisture stress indices (TSEB-SM) coupled to the evaporation and transpiration algorithm to estimate more accurately the soil evaporation and plant transpiration over study areas spanning well-watered to extremely dry soil moisture conditions.

Four in situ/tower-based micrometeorological and remote sensing observations were selected to evaluate both the TSEB-SM and original TSEB model. The sites included a rain fed grassland with seasonal soil moisture variation, irrigated cropland with no water stress during the growing season and an arid area with native vegetation, namely shrub-forest and desert steppe ecosystems, respectively. Finally, values of the ratio of T/ET partitioned by the TSEB-SM and TSEB models were compared with the values partitioned by *uWUE* (underlying water use efficiency) approach (Bai et al., 2019; Zhou et al., 2016) using the flux tower measurements over the grassland and irrigated cropland sites.

2. Materials and method

2.1. Sites and data

The meteorological and surface heat fluxes measurements were obtained from four flux towers which were deployed over grassland (2013–2017), irrigated cropland (2013–2017), sparse shrub-forest (2014–2017) and desert steppe (2014–2016) in the Heihe river basin (Fig. 1). The grassland site is located at A'rou (100.46° E, 38.05° N, 3033 m over the sea level) where the land surface is an alpine meadow, with an annual average air temperature and precipitation of 1 °C and 450 mm, respectively, but the potential evaporation is over 3500 mm. The irrigated cropland and desert steppe sites (100.37° E, 38.86° N, 1556 m above the sea level; 100.318° E, 38.765° N, 1731 m above the sea level) are located at Zhangye where the annual air temperature and precipitation are 7.3 °C and 130 mm, respectively, but the annual potential evaporation is 3200 mm. The shrub-forest site (101.14°E, 42.00°N, 873 m over the sea level) is located at E'jina is an arid area with average annual precipitation less than 50 mm but the potential evaporation is more than 4400 mm.

The sensible (H) and latent (LE) heat fluxes were measured by eddy covariance (EC) systems with a sampling frequency of 10 Hz and a description of the data post-processing can be found in Liu et al. (2018). The energy balance closure was enforced in these observations (H, LE, Rn (net radiation), G (soil heat flux)) by using the Bowen ratio approach (Twine et al., 2000). Closure ratios $(H + LE)/(Rn\text{-}G)$ for the sites were between 0.8 and 0.95. The ancillary meteorological measurements included air temperature, relative humidity, wind speed/direction and rain were measured by a weather station. The upward and downward solar and longwave radiations were measured using a four-component radiometer, which also was used to calculate the land surface temperature with estimates of the surface emissivity (Li et al., 2019). The soil moisture and temperature were measured at various depths (2, 4, 10, 20, 40, 80, 120, 160 cm) under the ground; here, the soil moisture measurement at 4 cm depth was used to calculate the soil stress factor for soil evaporation. Three heat transfer plates were buried at 6 cm with soil thermocouples above the plate for computing the heat storage term at each site for estimating the soil heat flux. Thus all four energy balance components, namely net radiation, soil heat flux and sensible and latent heat fluxes were measured at each of the sites (Liu et al., 2016; Liu et al., 2013; Xu et al., 2013). Another key input of leaf area index was obtained from 8-day 500 m MODIS LAI product (MOD15A2), which were temporally smoothed and gap-filled to the time-series data.

2.2. Models

Given current limitations in TSEB to estimate the T and E, respectively, the canopy transpiration and soil evaporation limited by soil can be adjusted by two factors related to canopy stomatal conductance ($\frac{g_{stress}}{g_a}$) and soil wetness factor (f_s):

$$T_c = T_a + \frac{Rn_c R_{ah}}{\rho c_p}\left(1 - \alpha_c f_g \frac{g_{stress}}{g_a}\frac{\Delta}{\Delta+\gamma}\right) \quad (1)$$

$$T_s = T_a + \frac{(Rn_s - G_0)(R_{ah} + R_s)}{\rho c_p}\left(1 - \alpha_s f_s \frac{\Delta}{\Delta+\gamma}\right) \quad (2)$$

Where Rn_c and Rn_s are the net radiation for soil and canopy and are initially calculated with T_c estimated as a minimum of T_a, air temperature at the reference height, and LST and T_s derived from Eq. (3) and are updated along with the new T_c and T_s, and R_{ah} is the aerodynamic resistance (s m^{-1}) to turbulent heat transport between the canopy source height and reference height of the wind and temperature measurements in the surface layer (see Norman et al., 1995). The symbol α_c is the Priestley-Taylor coefficient for the canopy and its value for the canopy transpiration under non-stressed conditions is assumed to be ~1.26

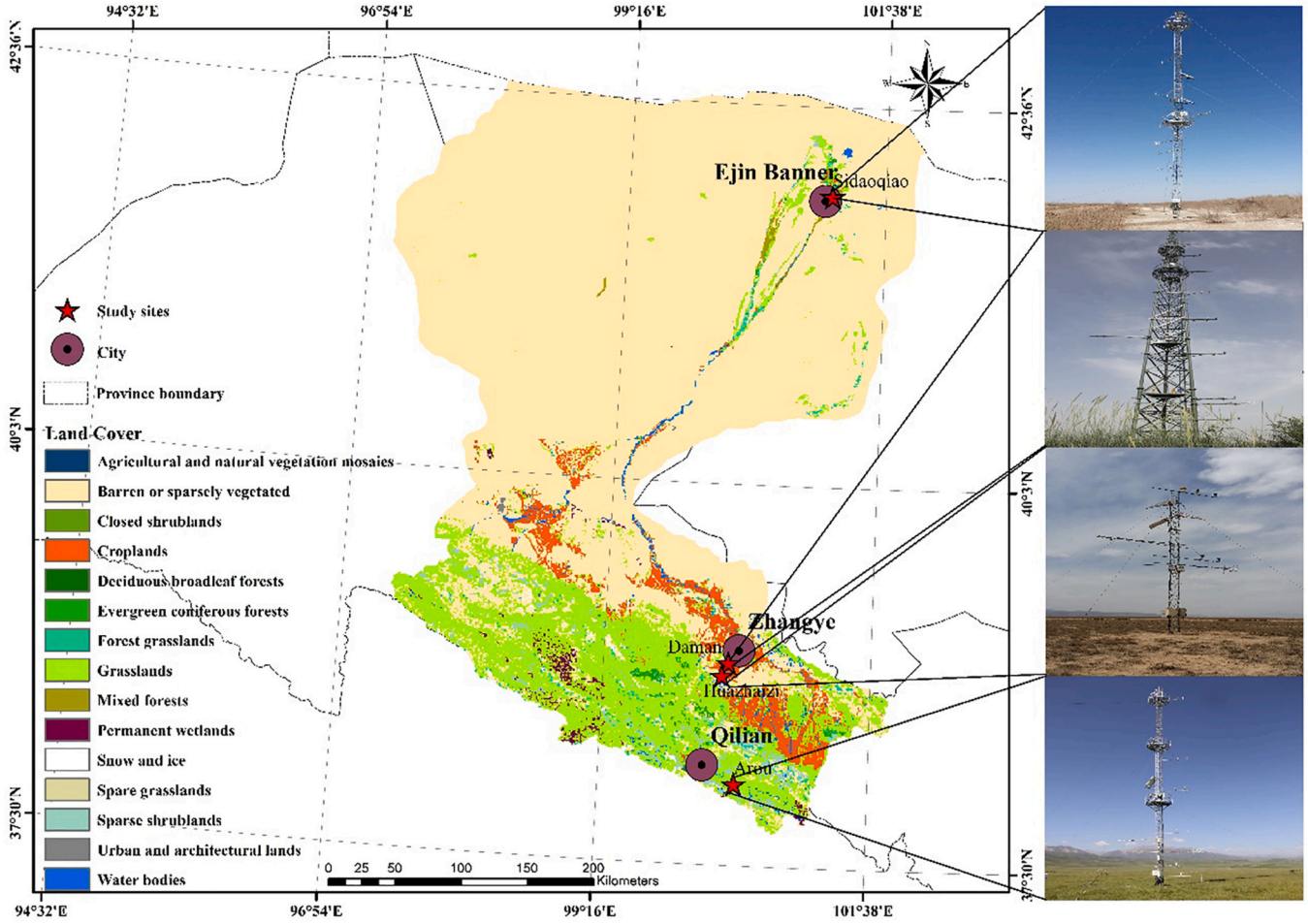

Fig. 1. Map of landcovers in Heihe river basin and EC flux tower sites at grassland, irrigated cropland and shrub-forest.

derived empirically by Priestley and Taylor (1972), f_g is the fraction of green vegetation which is able to transpire, $\frac{g_{stress}}{g_a}$ is the stress factor to the plant transpiration, Δ is the slope of the saturation vapor pressure versus air temperature curve (kPa K^{-1}) and γ is the psychometric constant of ~0.06 kPa K^{-1}. The value of f_g can be estimated using remote sensing (Fisher et al., 2008; Guzinski et al., 2013; Zhang et al., 2019). The resistance R_s is the soil aerodynamic resistance using the original formulation in TSEB (Norman et al., 1995), G_0 is surface soil heat flux, f_s is the factor of soil water stress which is used to adjust soil evaporation under drier surface soil moisture conditions, and α_s is the Priestley-Taylor coefficient applied to the soil. This differs from how TSEB uses the LST boundary condition by invoking the radiative temperature balance so that T_s and T_c must combine in Eq. (3) with fraction of vegetation coverage (f_c) to reproduce the radiometric temperature (T_{rad}) observation at the view angle.

$$T_{rad}^4(\theta) = f_c(\theta)T_c^4 + [1 - f_c(\theta)]T_s^4 \tag{3}$$

However, in TSEB-SM the final values of T_s and T_c from TSEB-SM may not aggregate to exactly match the LST in Eq. (3) as they are computed via Eqs. (1), (2) with updated Rn_c and Rn_s. Water stress acting on the soil evaporation can be expressed using the soil wetness factor for the decrease in the soil surface evaporation under the wet conditions. This soil moisture stress factor ($f_{s\text{-}song}$) had been introduced in TSEB model under irrigated agricultural field during the growing season, which can certainly improve the model performance (Song et al., 2016). While a similar factor ($f_{s\text{-}merlin}$) was proposed using an analytical approach (Merlin et al., 2011), which can be appropriately used under the dry conditions given the availability of the soil texture information.

However, the processes of water loss from soil surface may not be constrained adequately by $f_{s\text{-}song}$ under surface soil moisture conditions near or at field capacity leading to an underestimation in surface soil temperature (Fig. 2. a), while the $f_{s\text{-}merlin}$ has a greater constraint on soil evaporation over the full range in soil moisture content. Therefore a new stress function between $f_{s\text{-}song}$ and $f_{s\text{-}merlin}$ is defined for the full range of soil moisture content conditions using a multiplicative surface soil moisture stress factor (f_s) similar to the soil moisture stress module in GLEAM (Global Land Evaporation Amsterdam Model) (Martens et al., 2017). The multiplicative f_s can compensate for the limitations in the two stress factors, where the $f_{s\text{-}song}$ can underestimate the soil water constraint under relatively wet conditions and the $f_{s\text{-}merlin}$ causes greater stress under higher surface soil moisture content conditions. The new soil moisture stress factor is calculated as follows (Merlin et al., 2011; Song et al., 2016):

$$f_{s-song} = \frac{2}{1 + \left(\frac{\theta}{\theta_0}\right)^{-2}} \tag{4}$$

$$f_{s-merlin} = \frac{1}{2} - \frac{1}{2}cos\left(\frac{\theta}{\theta_{max}}\pi\right) \tag{5}$$

$$f_s = \sqrt{f_{s-song}f_{s-merlin}} \tag{6}$$

The value of $f_s = 1.0$ when soil moisture is greater than θ_{max}, where θ_0 is the wilting soil moisture content. To account for effect of the soil water content constraints on plant transpiration for short and tall vegetation explicitly, the canopy stomatal conductance stress factor,

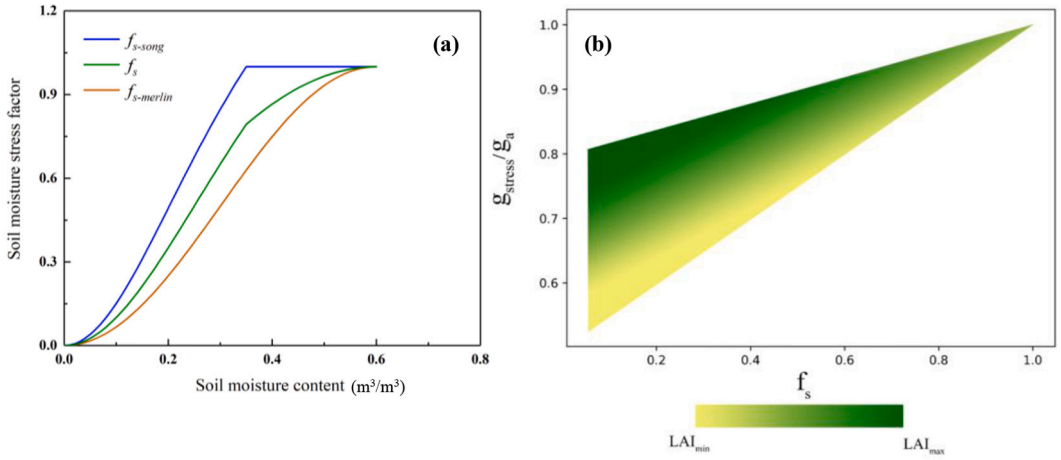

Fig. 2. Illustration of the soil moisture stress factor, fs, and canopy stomatal conductance stress functions implemented in TSEB-SM under various range of surface soil moisture content and vegetation cover conditions.

defined as a ratio between canopy stomatal conductance with and without water stress, is introduced to simulate the plant transpiration. The canopy stomatal conductance stress factor at ecosystem scale can be calculated as follows (De Kauwe et al., 2015; Kala et al., 2015):

$$\frac{g_{stress}}{g_a} = \frac{g_0{}^*LAI + 1.6\left(1 + \frac{g_1{}^*f_s}{\sqrt{VPD}}\right)\frac{A}{C_s}}{g_0{}^*LAI + 1.6\left(1 + \frac{g_1}{\sqrt{VPD}}\right)\frac{A}{C_s}} \quad (7)$$

where $g_0 = 0.01\ molH_2O\ m^{-2}s^{-1}$, is the leaf level minimum conductance which can be scaled from leaf to the canopy by accounting for LAI (leaf area index), $\boldsymbol{g_1}$ is a plant functional type dependent parameter which is set the same as used in CABLE (Community Atmosphere Biosphere Land Exchange) model; $\boldsymbol{C_s}$ and $\boldsymbol{VPD}$ are the CO_2 concentration and vapor pressure deficit, respectively. $\boldsymbol{A}$ is the leaf photosynthetic rate which can be calculated according to BEPS (Boreal Ecosystem Productivity Simulator) model (Chen et al., 1999; Qiu et al., 2019). As the soil moisture stress factor decreases, g_{stress}/g_a decreases, since water becomes less available for plant roots, but the falling rate of g_{stress}/g_a is also associated with the vegetation cover conditions (Fig. 2. b). The g_{stress}/g_a function is mainly defined both by surface moisture content and LAI. If the f_s and LAI both reach zero, the g_{stress}/g_a ratios equals zero. When f_s is zero but the LAI is high, the magnitude of g_{stress}/g_a is also large. Although only surface soil moisture information is contained in the ecosystem canopy stomatal conductance stress factor, the plant transpiration will more strongly correlate to the soil water content in the root zone. However, as seen from Eq. (5) and Fig. 2, when the LAI is low under sparse vegetation cover condition, g_{stress}/g_a mainly depends on surface soil moisture. On the contrary, when the LAI is large under dense vegetation cover conditions, g_{stress}/g_a has a weak correlation to surface soil moisture content.

Given the derived soil and canopy temperatures, the net radiation partitioned between the soil (Rn_s) and canopy (Rn_c) components can be calculated using the shortwave and longwave radiation divergence formulations of Kustas and Norman (1999). Then the sensible heat fluxes for soil (H_s) and canopy (H_c) surface can be calculated with the constraint of the soil (R_s) and canopy (R_x) aerodynamic resistances defined in Norman et al. (1995). With the energy balance equations of the soil and canopy surface, the soil (LE_s) and canopy (LE_c) latent heat flux can be calculated as the residual when the soil heat flux is considered as a fraction of Rn_s (Kustas and Anderson, 2009; Kustas and Norman, 1999).

2.3. Model validation

Compared with original TSEB model, the above framework not only uses the LST as an initial boundary condition but that can deviate from the radiative temperature balance constraint required by TSEB (Eq. 3) because it couples the soil moisture data into energy balance equation, TSEB-SM, and hence constrains both soil and canopy flux components. The new model was evaluated under a wide range of soil moisture content and environmental conditions with the meteorological measurements including LST, incoming shortwave radiation, wind speed, air temperature, atmosphere pressure, ambient CO_2 concertation at 3–5 m over the canopy, surface soil moisture measurement at 4 cm depth and satellite data of MODIS LAI with a spatial resolution of 500 m. Here, the model intercomparison of performance was quantified using the bias (average value of modeled outputs-measurements), mean absolute percent difference (MAPD, average of absolute difference between modeled outputs-measurements divvied by average measurements) and root mean square error (RMSE, square root of the sum of the differences between model outputs and measurements squared divided by the number of measurements).

Estimates of T and E partitioning were computed using the water use efficiency (uWUE) method. Details of the method can been found in Zhou et al. (2016). Briefly the canopy transpiration and CO_2 assimilation both across the leaf stomata, and was modeled using a stomatal conductance formulation (Beer et al., 2009). The water use efficiency at leaf scale was simulated as the ratio of gross primary productivity (GPP) and canopy transpiration associated with environmental forcing, primarily vapor pressure deficit (VPD). The water use efficiency for an ecosystem is described as the ratio of GPP and ET, which is a function of the local environment (Zhou et al., 2014; Zhou et al., 2016). The water use efficiency at leaf scale was assumed to be nearly constant for a particular ecosystem under steady state conditions. While the water use efficiency of an ecosystem can vary mainly due to the variation of non-stomatal direct evaporation from soil and wet canopy surfaces, the nearly constant water use efficiency at leaf scale allows the determination of water use efficiency using the quantile regression between the ET and the GPP multiplied by $VPD^{0.5}$ using all the half-hourly EC measurements. Hence with the EC measurements, the variability of water use efficiency for an ecosystem was derived from daily to monthly time scales (Bai et al., 2019; Zhou et al., 2014; Zhou et al., 2016). Finally, the ratio of the ecosystem water use efficiency and leaf water use efficiency was assumed to be indicative of the ratio T/ET.

3. Results

3.1. Models performance using EC flux measurements

The daytime half-hourly averaged meteorological and hemispherical LST data were used to run the TSEB and TSEB-SM which mainly require additional inputs of surface soil moisture data as a surrogate for microwave retrieval of surface soil moisture along with the MODIS LAI product to estimate the surface heat fluxes over different environmental conditions. Since the focus is on evaluation and comparison of the TSEB-SM model with ground measurements and original TSEB model, the measured and model results were first compared using half-hour fluxes. Then the modeled and measured *LE* values were accumulated during daytime and converted into *mm* for assessing the model performance for estimating daytime ET. Finally, the TSEB and TSEB-SM models partitioned T/ET were compared with the *uWUE* based method with EC measurements computed on a daytime basis during the growing season (DOY 153–273) since the vegetation is senescent during the no-growing season.

The agreement between the estimated and observed fluxes from the two models are acceptable over the selected period at the four sites over the wide range in environmental conditions, but better performance was obtained from the TSEB-SM model under low canopy cover conditions when the soil plays a more dominate role in the ET (cf. Figs. 3-5). This is particularly the case for the shrub-forest and desert steppe sites which remained under sparse vegetation cover (LAI < 1) over the whole growing season. This is likely due to the original soil resistance term in TSEB not being properly parameterized under sparse cover conditions as shown by Li et al. (2019). However, for the alpine meadow and irrigated cropland, one observes greater scatter and bias in all four energy balance components exists from both models under low cover conditions, which occurs primarily after the growing season when there is virtually no transpiration. This suggests other factors are not accounted for by both models related to the non-transpiring vegetation.

There is better agreement with the *LE* observations forcing closure using the TSEB-SM at the shrub-forest and desert steppe sites. For the shrub-forest site this is due to a lower bias in the estimate of *Rn* which is underestimated by TSEB. Interestingly, the bias is lower in G_0 and *H* for TSEB, but greater scatter and the underestimate in *Rn* leads to an underestimate (and bias) in *LE*. There is a known bias in the LAI product from MODIS under sparse canopy conditions (Song et al., 2018) which is likely to affect TSEB more than TSEB-SM since the T_s and T_c partitioning is strongly constrained by Eq. (3) for TSEB. For the desert steppe, the TSEB model overestimates *Rn*, causing an overestimate and G_0, which to some extent corrects for this overestimate, but *H* is underestimated which is likely to do with using the default coefficients in the soil aerodynamic resistance formulation used in TSEB as indicated by Li et al. (2019). The model error values of MAPD for *Rn* and *H* were slightly reduced at the meadow and cropland site but more significantly at the shrub-forest and desert steppe sites using the TSEB-SM model. The resulting impact on modeled *LE* was mainly an improvement using TSEB-SM at the shrub-forest and desert steppe sites with MAPD being reduced by 22% and 13%, respectively.

There are slightly greater errors in the TSEB-SM model output with ground measured G_0, with both models overestimating G_0 during the non-growing season. This likely because over the winter and early spring period the soil is typically frozen and consequently does not follow the assumed relationship with Rn_s used in the TSEB formulation. Furthermore, the surface soil heat fluxes were measured from three plates which have a very limited spatial sampling associated with the level of heterogeneity in the landscape and likely contribute to the significant scatter observed between the modeled and ground measured G_0. However, the relatively larger errors in estimating G_0 at the four sites do not adversely affect both TSEB model output of *LE* significantly due its value being relatively smaller than the other energy balance components, except during low canopy cover conditions, which occurs primarily during the non-growing season. However, this is not the case for the shrub-forest site where the impact of uncertainty in G_0 is larger.

3.2. Daily ET from models and observations

In Fig. 7, daily ET estimated from TSEB and TSEB-SM models are compared with EC observations from 2013 to 2017 for alpine meadow and irrigated cropland sites, from 2014 to 2017 for the arid shrub-forest

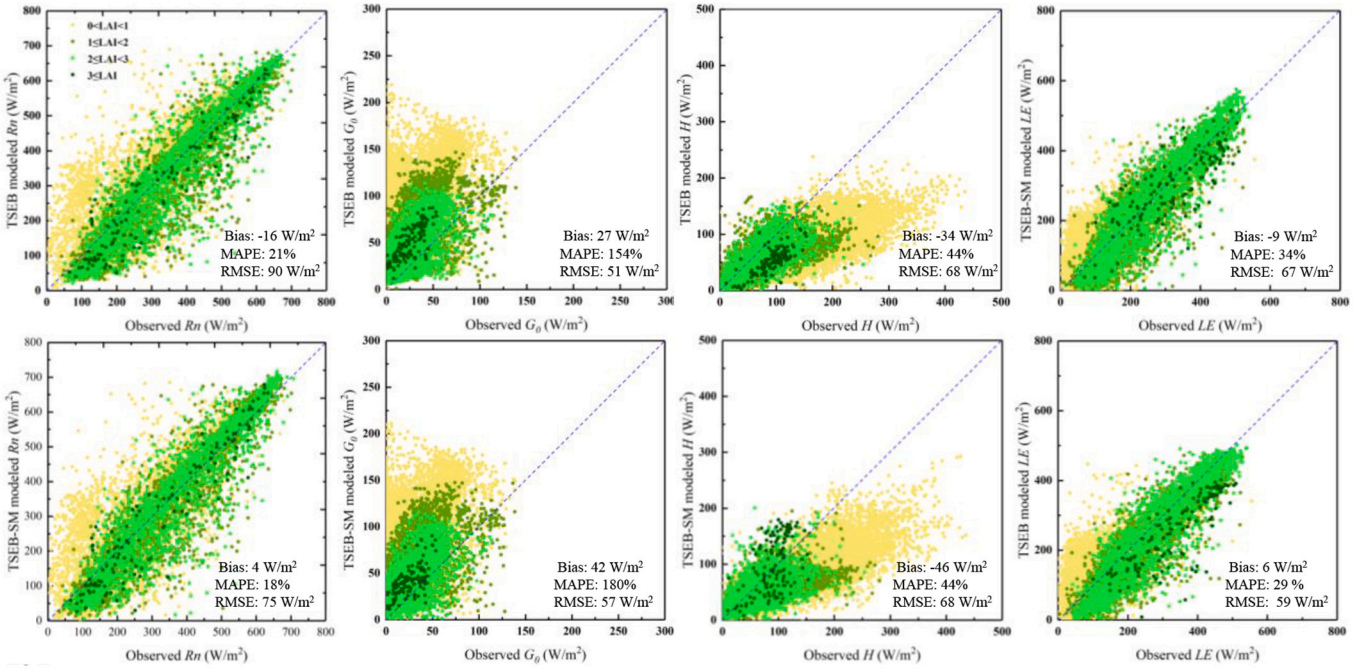

Fig. 3. Scatterplots of comparing measured half-hour net radiation, soil heat flux, sensible heat flux and latent heat flux from EC system and estimates from the TSEB and TSEB-SM models for the alpine meadow site.

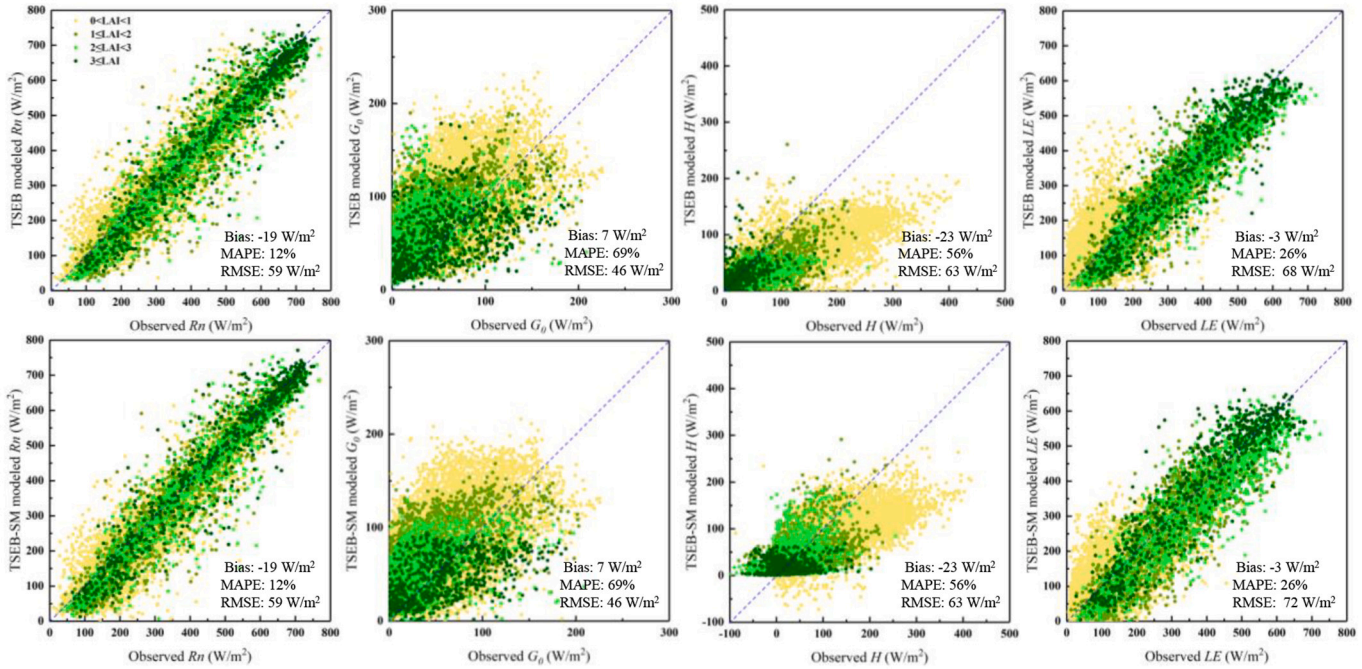

Fig. 4. Scatterplots of comparing measured half-hour net radiation, soil heat flux, sensible heat flux and latent heat flux from EC system and estimates from the TSEB and TSEB-SM models for the irrigated cropland site.

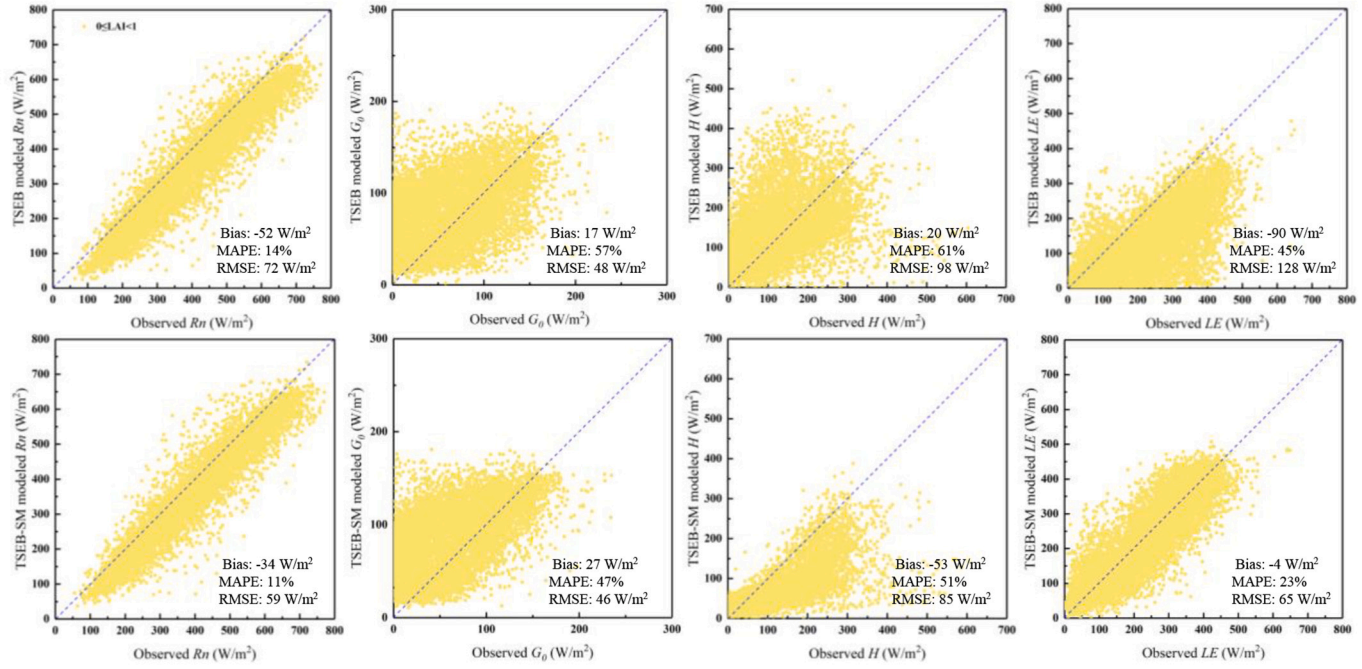

Fig. 5. Scatterplots of comparing measured half-hour net radiation, soil heat flux, sensible heat flux and latent heat flux from EC system and estimates from the TSEB and TSEB-SM models for shrub-forest site.

site and from 2014 to 2016 for the desert steppe site. As illustrated in Fig. 7 and the statistics in Table 1, the TSEB and TSEB-SM models performed similarly in the irrigated cropland site and grassland site, but the TSEB-SM model has significantly better agreement with the closed EC measurements at the shrub-forest and desert steppe sites, with MAPD reducing from 64% to 24% and from 52% to 40%, respectively. This is mainly due to the bias in daytime ET from TSEB under such low LAI conditions where, as illustrated in Figs. 5 and 6, the model biases particularly in *Rn*, and to some extent in *H* for the desert steppe site contribute to greater errors in daytime ET. However, Li et al. (2019) showed that when the soil aerodynamic resistance is properly parameterized for sparsely vegetated sites, TSEB can compute reliable and unbiased estimates of *H*. Note that both models overestimate daily ET under low LAI conditions for the alpine meadow and irrigated cropland sites, but tend to have a better agreement with ground measurements as the LAI values increase.

A temporal plot of daily modeled versus measured ET for 2014/2015 is illustrated in Figs. 8 through 11, a typical year with near continuous

Table 1
Statistical results of TSEB and TSEB-SM modeled vs EC system measured daily ET over alpine meadow, irrigated cropland and shrub-forest sites.

models	sites	Mean observed mm/day	MBE mm/day	MAPD (%)	RMSE mm/day
TSEB-SM	alpine meadow	1.86	0.01	25%	0.61
	irrigated cropland	2.00	−0.1	26%	0.71
	shrub-forest	1.51	−0.14	24%	0.50
	desert steppe	0.6	−0.15	40%	0.39
TSEB	alpine meadow		−0.13	28%	0.69
	irrigated cropland		−0.17	26%	0.73
	shrub-forest		−0.93	64%	1.31
	desert steppe		0.26	52%	0.48

EC measurements. Both modeled and observed daily ET show similar temporal patterns for all three sites. Daily ET values are low and stable for a prolong period before crop emergence in the irrigated cropland and leaf out for the mixed shrub forested sites by early April (DOY ~100) as indicated in Figs. 9 and 10. The values increase gradually in the early May (~DOY 150) and then increase rapidly, reaching maximum daily ET values by mid-July. The values decease gradually starting by the end of July (DOY ~215) as plants mature and then begin to go into senescent stage, resulting in a steady decrease in daily ET, which is further amplified after the first frost typically in September. Finally, the daily values become extremely low after vegetation has undergone senescence with frozen soils, over the winter.

The two modeled ET can track the yearly dynamics of the water consumption measured by the EC systems, the ET values varied along with the variation of daily incoming shortwave radiation and soil moisture content. However, the two models both underestimated the daily ET in the peak of growing season and the periods following heavy rainfall events which is due in part to the lack of being able to estimate evaporation from plant intercepted water. These discrepancies due to rain events contributing to the bias and MAPD statistics. The flood irrigation and heavy rain events can rapidly elevate the soil moisture content and the values can sometimes exceed the field capacity. The daily ET yielded by the TSEB exhibit a slight departure from the ground measurements under these saturated soil conditions (Figs. 9 and 11).

Figs. 12 and 13 illustrate the comparison of daily T/ET computed with TSEB and TSEB-SM models versus the *uWUE* method and the associated trend of LAI during the growing season in grassland and irrigated cropland sites from 2013 to 2017, respectively. As expected, the temporal trend in computed daily T/ET follows the temporal variations of LAI in the irrigated crop land during the growing season. However, the daily values of T/ET fluctuate with the variation in daily incoming shortwave radiation. The TSEB-SM model produced lower T/ET values compared with TSEB model but is in better agreement with the values computed by the *uWUE* method. The *uWUE* method computed larger magnitudes of T/ET values on clear days versus cloudy or rainy days. The large divergence in daily T/ET produced by the TSEB model may not only be related to the energy partitioning being strongly dependent on the LAI value (Kustas et al., 2019) but also on the fraction green *fg*, more so than with TSEB-SM having a soil moisture-based transpiration algorithm. For the cropland in the early season, the maize seedlings emerge, but has minimal contribution to *T*, resulting in a low T/ET value. Then, T/ET values increase rapidly as the maize crop develops increasing LAI. By the middle of July (~DOY 190), the cropland features transpiring maize at nearly 100% canopy cover. As the T/ET values reach near unity particularly during sunny days with high canopy cover, there begins a gradual decline from late July through August (DOY 190–245) when the maize cobs start filling and green LAI decreases. The downward trend of T/ET is further amplified as the crop goes through senescence and harvest (September, DOY 246–273) at the irrigated crop site and the grass undergoes senescence at the meadow/grassland site. This is the period where the T/ET is significantly overestimated by TSEB which is likely caused by the lack of accurate *fg* values. This affect does not seem to be apparent with the TSEB-SM model, which maybe due to the fact that in this period, the rapid decline of LAI which affects the transpiration algorithm in TSEB-SM and more accurate soil *E* results in a more reliable T/ET ratio.

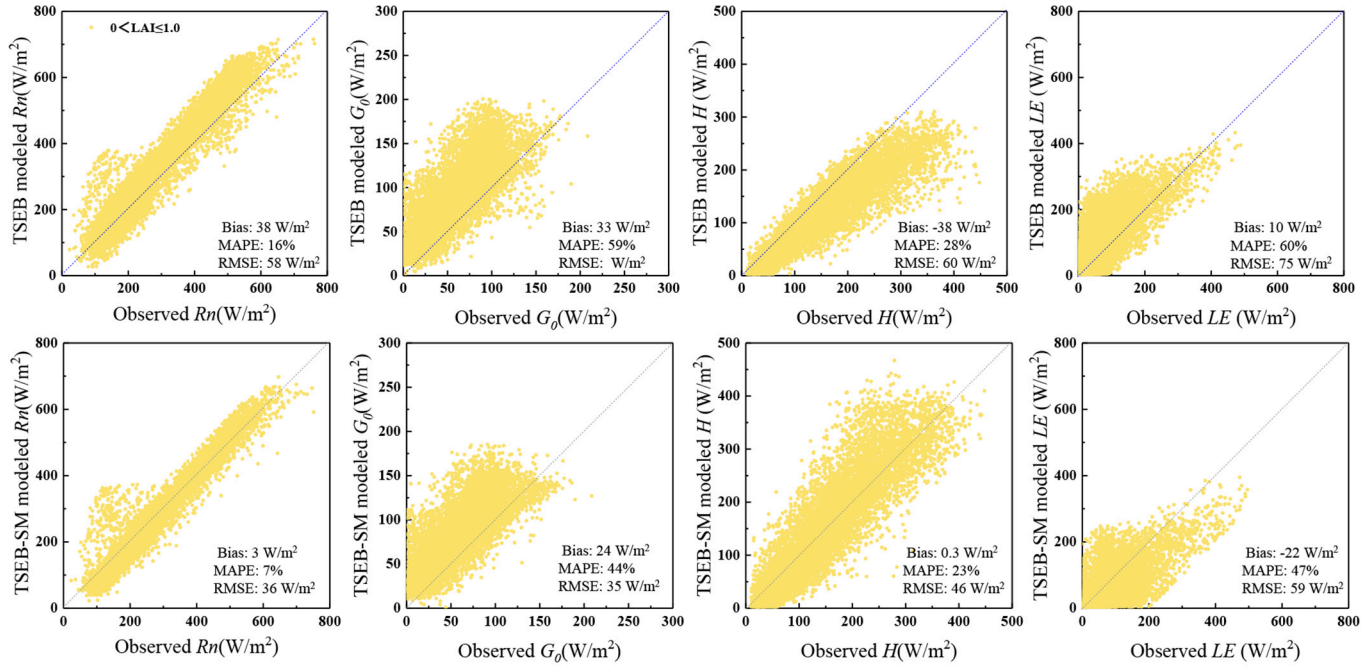

Fig. 6. Scatterplots of comparing measured half-hour net radiation, soil heat flux, sensible heat flux and latent heat flux from EC system and estimates from the TSEB and TSEB-SM models for desert steppe site.

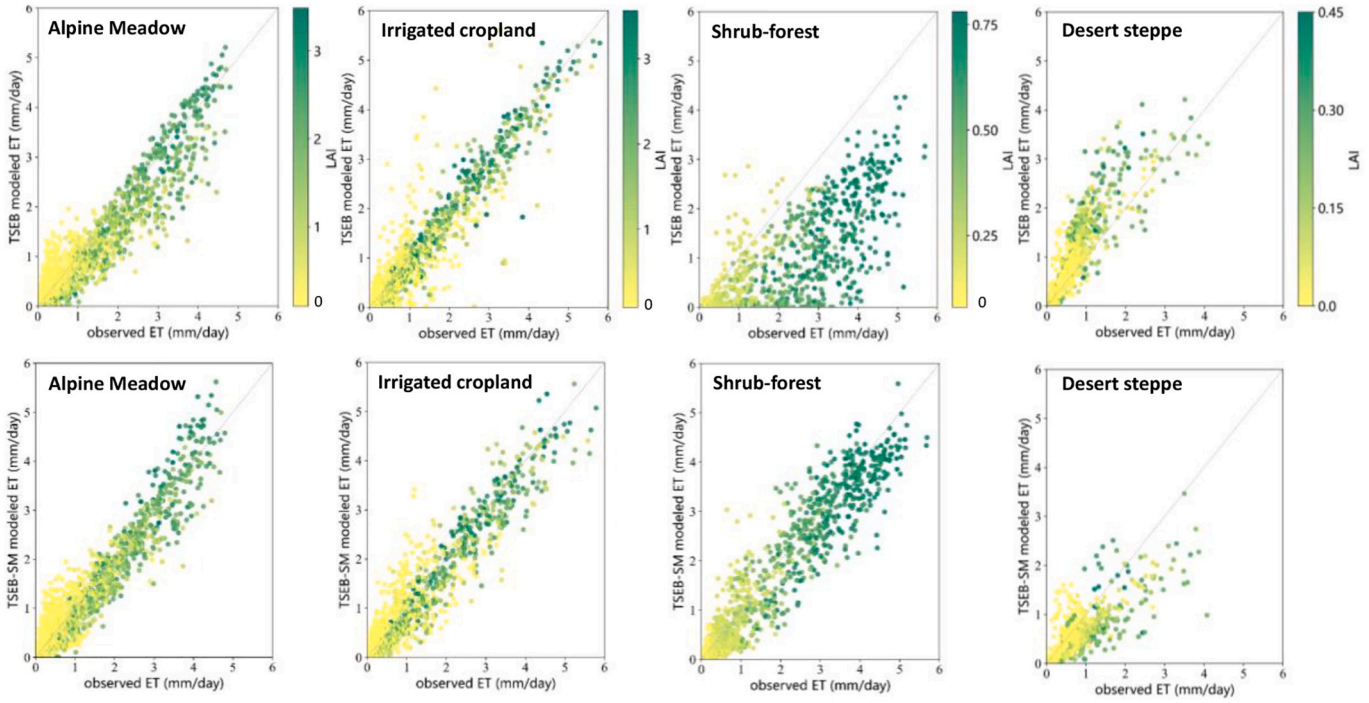

Fig. 7. Scatterplots of comparing measured daily ET from EC system and estimates from the TSEB and TSEB-SM models.

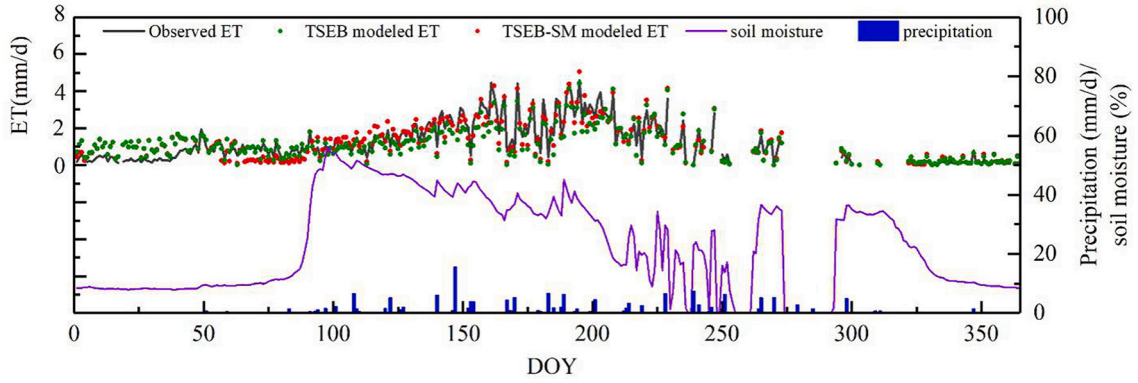

Fig. 8. Daily ET estimated from TSEB and TSEB-SM models compared with measurements from EC system at grassland site for 2015.

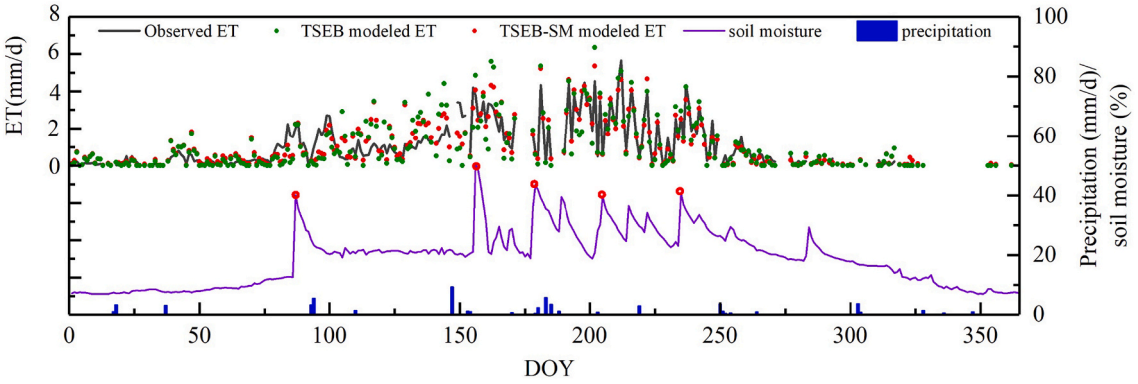

Fig. 9. Daily ET estimated from TSEB and TSEB-SM models compared with measurements from EC system at irrigated cropland site for 2015.The red circles represent the flood irrigation events. (For interpretation of the references to colour in this figure legend, the reader is referred to the web version of this article.)

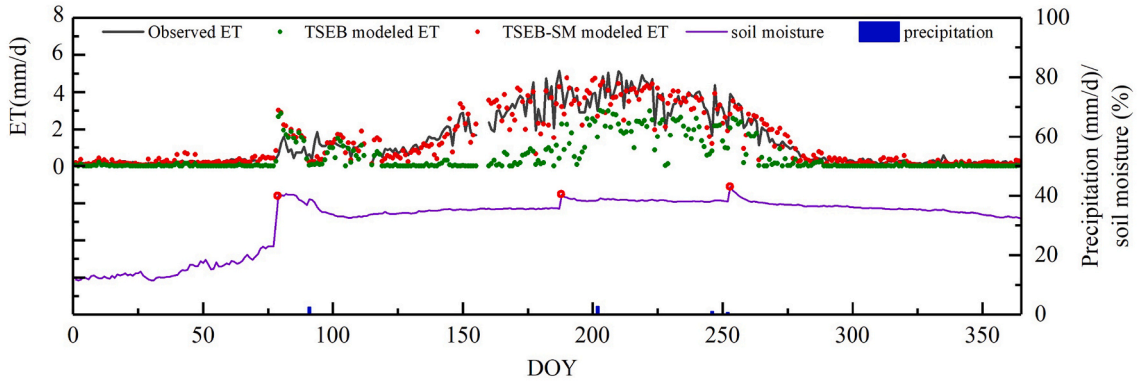

Fig. 10. Daily ET estimated from TSEB and TSEB-SM models compared with measurements from EC system at shrub-forest site for 2015. The red circle represents a major flood irrigation event that always is conducted in the Spring. (For interpretation of the references to colour in this figure legend, the reader is referred to the web version of this article.)

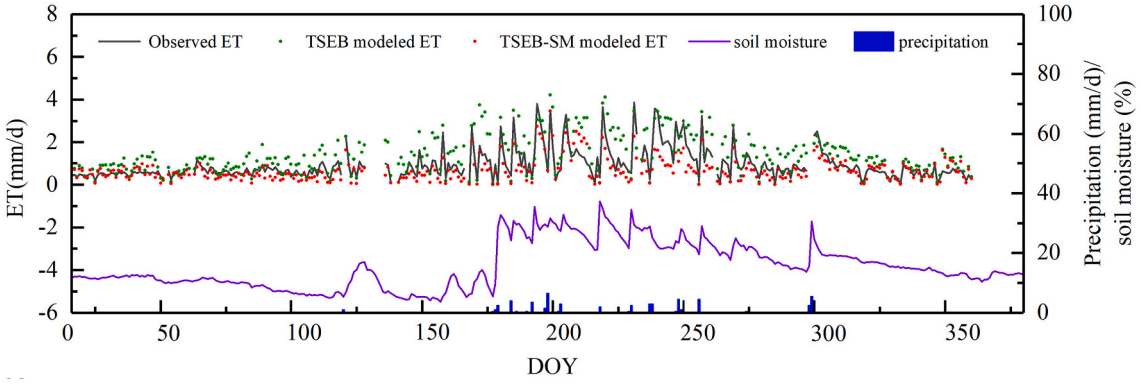

Fig. 11. Daily ET estimated from TSEB and TSEB-SM models compared with measurements from EC system at desert steppe site for 2014.

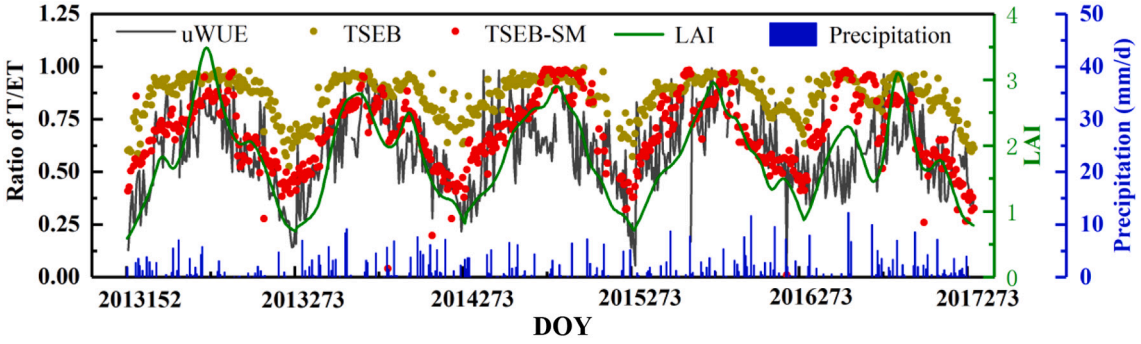

Fig. 12. Daily ratio between *T* and *ET* separated from TSEB and TSEB-SM models compared with partitioning using *u*WUE method from EC measurements at grassland site during growing season in 2013–2017.

4. Discussion

The TSEB-SM model estimated more reliable *E* and *T* partitioning over the grassland and cropland sites based on the *uWUE* method while significantly better agreement in modeled-measured daily ET for the forest-shrub and desert steppe sites. The maximum divergence of the *T/ET* estimated from the two models appeared during the period of decreasing vegetation cover/leaf area as the fraction of green actively transpiring vegetation decreases as plants undergo seed development and ripening, especially towards the end of the growing season. The two models both can provide the temporal behavior of increased *T/ET* along with the plant growth indicated by the variation of LAI values. These seasonal trends have smaller day-to-day fluctuations when compared with the results partitioned from the *uWUE* approach. Additionally, the two models also can respond to the dynamics of the environmental conditions such as the rainfall events, where the modeled *T* declined rapidly. Finally, the canopy stress factor introduced in the TSEB-SM model can provide a reasonable constraint on the daily *T* value when the plant water use is limited using the near surface soil moisture in combination of environmental factors. TSEB model has a larger T/ET ratio than the *u*WUE and TSEB-SM model estimates during the latter part of the growing season. This may be associated with the soil and vegetation flux partitioning in TSEB model is strongly dependent on the *fg* along with the magnitude in LAI. The errors in estimating *fg* tend to increase later in the growing season when the senescent leaves do not contribute to *T*, while satellite spectral sensors mainly detect green

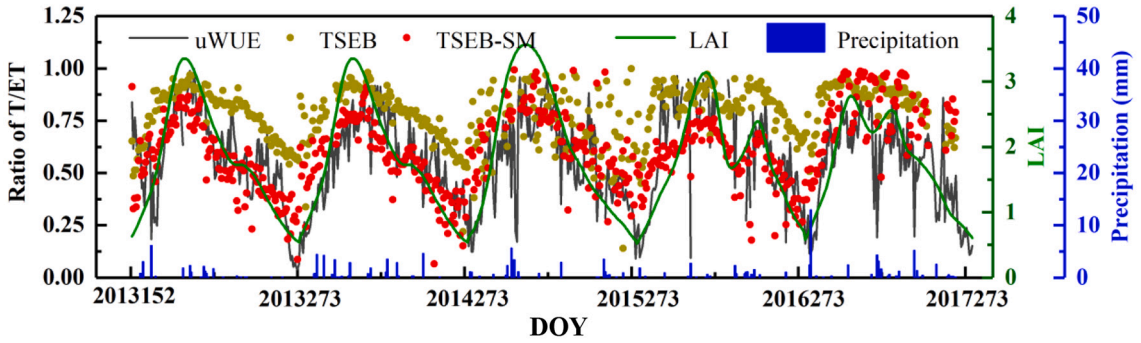

Fig. 13. Daily ratio between *T* and *ET* separated from TSEB and TSEB-SM models compared with partitioning using uWUE method from EC measurements at irrigated cropland site during growing season in 2013–2017.

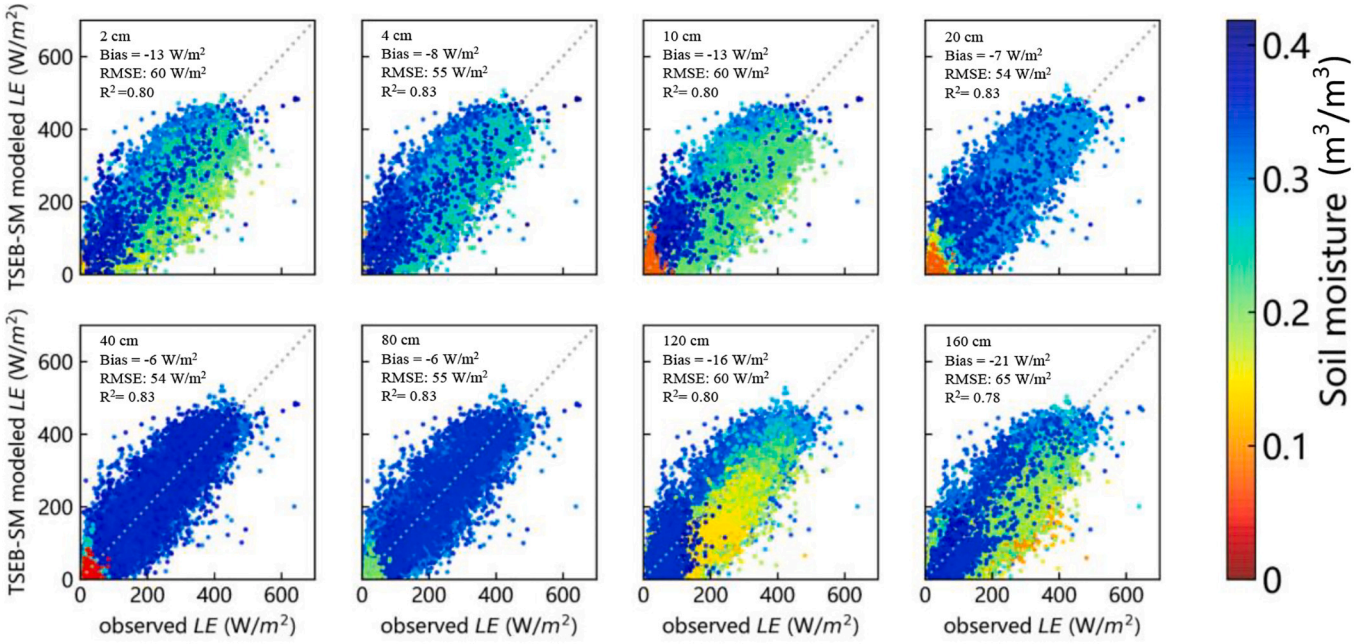

Fig. 14. Scatterplots of comparing measured half-hour latent heat flux from EC system and estimates from the TSEB-SM model with soil moisture data measured from surface to root zone (2, 4, 10, 20, 40, 80, 120, 160 cm) at the shrub forest site.

actively transpiring vegetation and hence cannot easily provide reliable *fg* values.

The *E* presented an opposite temporal trend with *T*, as *E* would have significant variation early in the growing season from wetting and drying cycles due to precipitation but declined gradually as the plants grew/greened up and increased in leaf area. This decrease was due in part to the increased vegetation coverage resulting in less radiation reaching the soil surface under the canopy layer and reduced wind and turbulent exchange. The two models provided similar *E* values for the irrigated cropland site, but the TSEB-SM model produced higher *E* values at shrub-forest and desert steppe sites with sparse vegetation cover, which increased the daily ET contribution from the soil and thus reduced the underestimation of ET. For the shrub-forest site, the periodic flood irrigations to mitigate tree stress and maintain growth during extended periods of hot and dry conditions results in a high surface soil moisture content which appears to be replenished by upward movement of available water from deeper layers in between irrigation events. Additionally, there is a salt crust at the soil surface which likely affected application of the standard soil aerodynamic resistance used in TSEB (Li et al., 2019). Moreover, observed cracks in the salt crust on the soil surface would be a significant source of *E* given the wet soil surface moisture conditions throughout the growing season (Fig. 10) while the salt crust would cause elevated soil temperatures using TSEB resulting in an underestimate in *E*. In addition, field measurements of LAI at the shrub-forest site indicates that the MODIS LAI product underestimated the actual LAI within the smaller source area of flux tower by approximately 50% contributing to the underestimate by TSEB. However, even with a LAI increase there is still a significant soil contribution so the results with TSEB are not significantly improved with increasing LAI (not shown).

The soil water content at root zone is assumed to be a greater constraint on ET than the surface soil due to the fact that plant transpiration is closely tied to plant available water in the root zone However, this relationship varies with the vegetation type, phenology, season and root distribution (Qiu et al., 2020). The surface soil moisture also contains information that can be related to deeper soil moisture conditions. Additionally, observations of the root zone soil moisture at regional scales do not exist at fine enough resolution to be used in mapping ET whereas the near-surface soil water content can be mapped from the microwave observations (Entekhabi et al., 2010). Therefore, in this study the plant transpiration constraining factor, g_{stress}/g_a, is defined according to the vegetation growth, surface soil moisture and

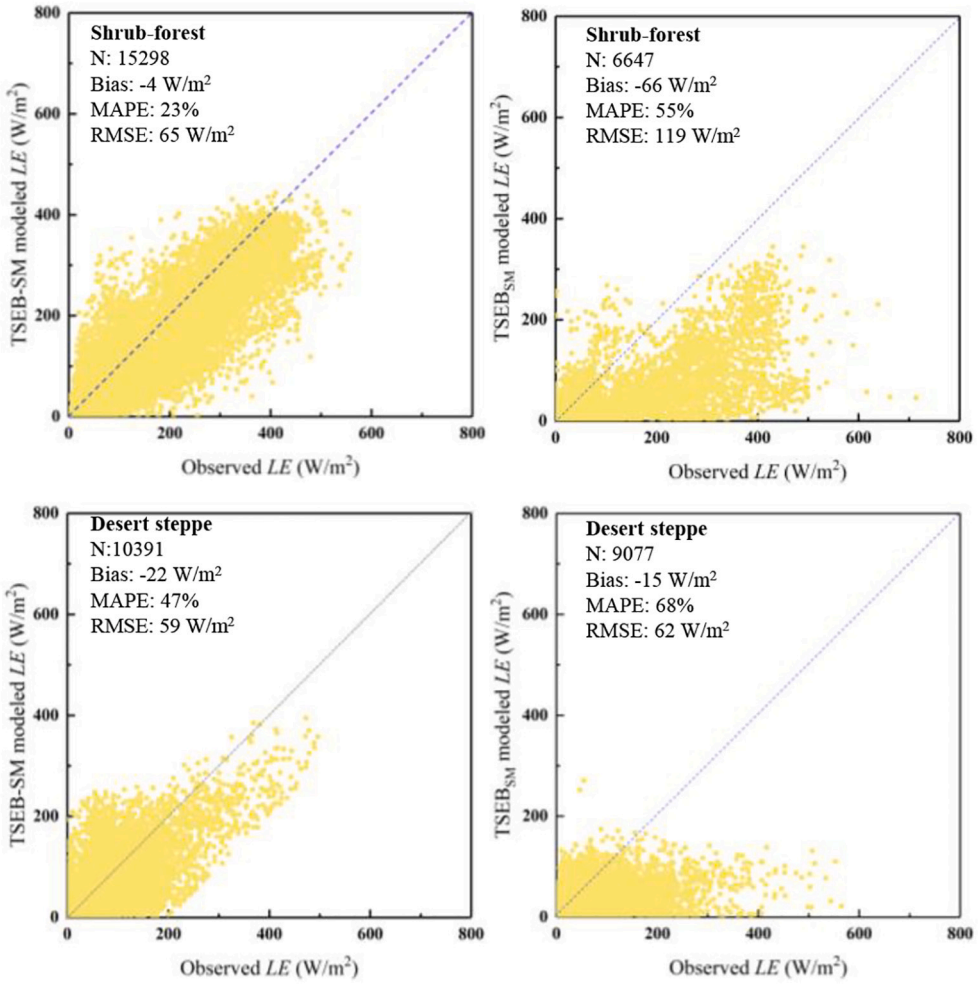

Fig. 15. Scatterplots of comparing measured half-hour latent heat flux from EC system and estimates from the TSEB-SM, and Penman-Monteith models for shrub-forest and desert steppe site.

environmental conditions and combined with land surface temperature to provide an improved metric of surface and root zone water availability. The formulation is shown to compute reliable ET for the shrub-forest and desert steppe semi-arid sites where the vegetation is adapted for water limited conditions but can still be stressed. To evaluate the performance of g_{stress}/g_a using the surface soil water content as input, the soil moisture measured at various vertical depths (2, 4, 10, 20, 40, 80, 120, 160 cm) at the shrub-forest site were used as input to the g_{stress}/g_a formulation then the modeled *LE* values from the TSEB-SM were compared to the ground measurements (Fig. 14). The TSEB-SM model performances were quite similar when using the soil moisture measurements at 4, 20, 40, and 80 cm as input to g_{stress}/g, with RMSE values all around 55–60 W/m^2 except when using the water content at 160 cm, which produced an RMSE value slightly higher at 65 W/m^2. These results suggest that the g_{stress}/g using near-surface soil moisture as input can perform similarly to water content values in the root zone at least for the site and conditions evaluated in this study. As mentioned, the g_{stress}/g function is mainly determined by the LAI, near-surface soil moisture and VPD, which are metrics of the plant phenology, soil water availability and the atmosphere demand, respectively. These parameters influence the canopy stomatal closure which when combined with land surface temperature better determine the variation of plant transpiration.

To compare the performance of TSEB-SM model with another widely used ET model, the Penman-Monteith algorithm was applied at the shrub-forest and desert steppe sites. The results showed that TSEB-SM outperform this modeling approach.

The Penman-Monteith algorithm gave very poor results for estimating LE at shrub-forest site and the desert steppe site. Without a priori calibration, the Penman-Monteith algorithm has difficulty reproducing the ET in these semi-arid environments (Zhang et al., 2019).

The TSEB-SM model proposed in this study can provide reliable estimation of ET under the sparse vegetation cover and dry soil surface (Figs. 5, 6 and 15) and can produce similar results with the TSEB model over the denser vegetation cover and wetter soil surface (Figs. 3 and 4). It also can yield a more consistent in ET partitioning than TSEB model when compared with the *uWUE* approach separated results using the flux tower measurements (Figs. 12 and 13).

5. Conclusions

A new algorithm using surface soil moisture data to constrain soil evaporation coupled to a new transpiration algorithm containing a stomatal resistance-based stress factor was introduced into the TSEB model (TSEB-SM) to generate ET in a semi-arid region over four different land covers, irrigated cropland, grassland a sparsely vegetated shrub-forest and desert steppe ecosystem. The TSEB-SM was assessed using the flux tower based EC measurements with forced closure over multiple growing seasons, and was compared with the performance of original TSEB model. The estimated surface fluxes from TSEB-SM yielded generally better agreement with ground measurements for the shrub-forest and desert steppe sites in *Rn* and *LE* but yielded no real improvement for the cropland and grassland or meadow site, except

under low canopy cover/non-growing conditions.

The TSEB-SM model computed more reliable fluxes than TSEB when the canopy cover is low or non-existent and for the shrub-forest site throughout the year (Fig. 5) suggesting that the soil aerodynamic resistance formulation is not properly parameterized for these arid ecosystems (Li et al., 2019) and that the significant underestimation of LAI using MODIS also affects the roughness and hence soil and canopy aerodynamic resistance terms. Moreover, the bias in the estimated net radiation from TSEB is a significant factor, which could be improved with more reliable soil albedo estimates. The seasonal trends in T/ET over the grassland and irrigated cropland sites produced by the TSEB and TSEB-SM models both follow the temporal trend in LAI, but it appears that TSEB-SM generally has better agreement with T/ET estimated using the *uWUE* method. The largest disagreement in T/ET between TSEB-SM and TSEB is in the period of cropland/grassland senescence as the green LAI decreases (Figs. 10 and 11) suggesting the *fg* was not properly prescribed in TSEB. The TSEB-SM with a different transpiration formulation is not as sensitive to the value of *fg*.

The TSEB-SM model requires additional inputs of soil moisture data which are being produced using the observations from active microwave sensors (Sentinel-1) or by combining the microwave soil moisture data and a data fusion approach. However, the accuracy of these high-resolution soil and soil moisture data may need further refinement to be applicable to monitoring ET. Additionally, sun-introduce chlorophyll fluorescence (SIF) data have potential to provide information on plant transpiration useful in defining the parameters for the proposed transpiration algorithm and as a metric or indicator of the soil moisture status at the root zone (Jonard et al., 2020). SIF has the potential to further constrain TSEB model transpiration estimates resulting in both an improved daily ET and T/ET partitioning. However, the spatially and temporally sparse data supplied by the current sensors is challenge for field scale applications.

Credit author statement

L. S. designed the study and wrote the article with the support from W. P. K. L. S. performed the analyses with additional support from Z. D., G. Z. and K. X. on data processing and drawing. S. L. and Z. X. provided the ground measurements. All authors contributed to edited the manuscript.

Declaration of Competing Interest

The authors declare that they have no known competing financial interests or personal relationships that could have appeared to influence the work reported in this paper.

Acknowledgement

This work was supported by the National Natural Science Foundation of China (42071298, 41701377). This research was supported in part by the U.S. Department of Agriculture, Agricultural Research Service. Mention of trade names or commercial products in this publication is solely for the purpose of providing specific information and does not imply recommendation or endorsement by the U.S. Department of Agriculture. USDA is an equal opportunity provider and employer.

References

Agam, N., Evett, Steven R., Tolk, Judy A., Kustas, William P., Colaizzi, Paul D., Alfieri, Joseph G., Mckee, Lynn G., Copeland, Karen S., Howell, Terry A., Chávez, Jose L., 2012. Evaporative loss from irrigated interrows in a highly advective semi-arid agricultural area. Adv. Water Resour. 50, 20–30. https://doi.org/10.1016/j.advwatres.2012.07.010.

Ait Hssaine, B., Merlin, O., Rafi, Z., Ezzahar, J., Jarlan, L., Khabba, S., Er-Raki, S., 2018. Calibrating an evapotranspiration model using radiometric surface temperature, vegetation cover fraction and near-surface soil moisture data. Agric. For. Meteorol. 256-257, 104–115.

Ait Hssaine, B., Chehbouni, A., Er-Raki, S., Khabba, S., Ezzahar, J., Ouaadi, N., Ojha, N., Rivalland, V., Merlin, O., 2021. On the utility of high-resolution soil moisture data for better constraining thermal-based energy balance over three semi-arid agricultural areas. Remote Sens. 13, 727.

Anderson, M.C., Norman, J.M., Kustas, W.P., Houborg, R., Starks, P.J., Agam, N., 2008. A thermal-based remote sensing technique for routine mapping of land-surface carbon, water and energy fluxes from field to regional scales. Remote Sens. Environ. 112, 4227–4241.

Bai, Y., Li, X., Zhou, S., Yang, X., Yu, K., Wang, M., Liu, S., Wang, P., Wu, X., Wang, X., Zhang, C., Shi, F., Wang, Y., Wu, Y., 2019. Quantifying plant transpiration and canopy conductance using eddy flux data: an underlying water use efficiency method. Agric. For. Meteorol. 271, 375–384.

Beer, C., Ciais, P., Reichstein, M., Baldocchi, D., Law, B.E., Papale, D., Soussana, J.-F., Ammann, C., Buchmann, N., Frank, D., Gianelle, D., Janssens, I.A., Knohl, A., Köstner, B., Moors, E., Roupsard, O., Verbeeck, H., Vesala, T., Williams, C.A., Wohlfahrt, G., 2009. Temporal and among-site variability of inherent water use efficiency at the ecosystem level. Glob. Biogeochem. Cycles 23.

Brust, C., Kimball, J.S., Maneta, M.P., Jencso, K., He, M., Reichle, R.H., 2021. Using SMAP Level-4 soil moisture to constrain MOD16 evapotranspiration over the contiguous USA. Remote Sens. Environ. 255, 112277.

Chen, J.M., Liu, J., Cihlar, J., Goulden, M.L., 1999. Daily canopy photosynthesis model through temporal and spatial scaling for remote sensing applications. Ecol. Model. 124, 99–119.

Colaizzi, P.D., Kustas, W.P., Anderson, M.C., Agam, N., Tolk, J.A., Evett, S.R., Howell, T. A., Gowda, P.H., O'Shaughnessy, S.A., 2012. Two-source energy balance model estimates of evapotranspiration using component and composite surface temperatures. Adv. Water Resour. 50, 134–151.

De Kauwe, M.G., Kala, J., Lin, Y.S., Pitman, A.J., Medlyn, B.E., Duursma, R.A., Abramowitz, G., Wang, Y.P., Miralles, D.G., 2015. A test of an optimal stomatal conductance scheme within the CABLE land surface model. Geosci. Model Dev. 8, 431–452.

Entekhabi, D., Njoku, E.G., Neill, P.E.O., Kellogg, K.H., Crow, W.T., Edelstein, W.N., Entin, J.K., Goodman, S.D., Jackson, T.J., Johnson, J., Kimball, J., Piepmeier, J.R., Koster, R.D., Martin, N., McDonald, K.C., Moghaddam, M., Moran, S., Reichle, R., Shi, J.C., Spencer, M.W., Thurman, S.W., Tsang, L., Zyl, J.V., 2010. The soil moisture active passive (SMAP) mission. Proc. IEEE 98, 704–716.

Fisher, J.B., Tu, K.P., Baldocchi, D.D., 2008. Global estimates of the land–atmosphere water flux based on monthly AVHRR and ISLSCP-II data, validated at 16 FLUXNET sites. Remote Sens. Environ. 112, 901–919.

Gan, G., Gao, Y., 2015. Estimating time series of land surface energy fluxes using optimized two source energy balance schemes: model formulation, calibration, and validation. Agric. For. Meteorol. 208, 62–75.

Guzinski, R., Anderson, M.C., Kustas, W.P., Nieto, H., Sandholt, I., 2013. Using a thermal-based two source energy balance model with time-differencing to estimate surface energy fluxes with day-night MODIS observations. Hydrol. Earth Syst. Sci. Discuss. 10, 1897–1941.

Houborg, R., Anderson, M.C., Daughtry, C.S.T., Kustas, W.P., Rodell, M., 2011. Using leaf chlorophyll to parameterize light-use-efficiency within a thermal-based carbon, water and energy exchange model. Remote Sens. Environ. 115, 1694–1705.

Jonard, F., De Cannière, S., Brüggemann, N., Gentine, P., Short Gianotti, D.J., Lobet, G., Miralles, D.G., Montzka, C., Pagán, B.R., Rascher, U., Vereecken, H., 2020. Value of sun-induced chlorophyll fluorescence for quantifying hydrological states and fluxes: current status and challenges. Agric. For. Meteorol. 291, 108088.

Jung, M., Reichstein, M., Ciais, P., Seneviratne, S.I., Sheffield, J., Goulden, M.L., Bonan, G., Cescatti, A., Chen, J., de Jeu, R., Dolman, A.J., Eugster, W., Gerten, D., Gianelle, D., Gobron, N., Heinke, J., Kimball, J., Law, B.E., Montagnani, L., Mu, Q., Mueller, B., Oleson, K., Papale, D., Richardson, A.D., Roupsard, O., Running, S., Tomelleri, E., Viovy, N., Weber, U., Williams, C., Wood, E., Zaehle, S., Zhang, K., 2010. Recent decline in the global land evapotranspiration trend due to limited moisture supply. Nature 467, 951–954.

Kala, J., De Kauwe, M.G., Pitman, A.J., Lorenz, R., Medlyn, B.E., Wang, Y.P., Lin, Y.S., Abramowitz, G., 2015. Implementation of an optimal stomatal conductance scheme in the Australian Community Climate Earth Systems Simulator (ACCESS1.3b). Geosci. Model Dev. 8, 3877–3889.

Kustas, W., Anderson, M., 2009. Advances in thermal infrared remote sensing for land surface modeling. Agric. For. Meteorol. 149, 2071–2081.

Kustas, W.P., Norman, J.M., 1999. Evaluation of soil and vegetation heat flux predictions using a simple two-source model with radiometric temperatures for partial canopy cover. Agric. For. Meteorol. 94, 13–29.

Kustas, W.P., Bindlish, R., French, A.N., Schmugge, T.J., 2003a. Comparison of energy balance modeling schemes using microwave-derived soil moisture and radiometric surface temperature. Water Resour. Res. 39, 1039.

Kustas, W.P., Bindlish, R., French, A.N., Schmugge, T.J., 2003b. Comparison of energy balance modeling schemes using microwave-derived soil moisture and radiometric surface temperature. Water Resour. Res. 39.

Kustas, W.P., Anderson, M.C., Alfieri, J.G., Knipper, K., Torres-Rua, A., Parry, C.K., Nieto, H., Agam, N., White, W.A., Gao, F., McKee, L., Prueger, J.H., Hipps, L.E., Los, S., Alsina, M.M., Sanchez, L., Sams, B., Dokoozlian, N., McKee, M., Jones, S., Yang, Y., Wilson, T.G., Lei, F., McElrone, A., Heitman, J.L., Howard, A.M., Post, K., Melton, F., Hain, C., 2018. The grape remote sensing atmospheric profile and evapotranspiration experiment. Bull. Am. Meteorol. Soc. 99, 1791–1812.

Kustas, W.P., Alfieri, J.G., Nieto, H., Wilson, T.G., Gao, F., Anderson, M.C., 2019. Utility of the two-source energy balance (TSEB) model in vine and interrow flux partitioning over the growing season. Irrig. Sci. 37, 375–388.

Li, M., Zhou, J., Peng, Z., Liu, S., Göttsche, F.-M., Zhang, X., Song, L., 2019. Component radiative temperatures over sparsely vegetated surfaces and their potential for upscaling land surface temperature. Agric. For. Meteorol. 276-277, 107600.
Liu, S.M., Xu, Z.W., Zhu, Z.L., Jia, Z.Z., Zhu, M.J., 2013. Measurements of evapotranspiration from eddy-covariance systems and large aperture scintillometers in the Hai River Basin, China. J. Hydrol. 487, 24–38.
Liu, S., Xu, Z., Song, L., Zhao, Q., Ge, Y., Xu, T., Ma, Y., Zhu, Z., Jia, Z., Zhang, F., 2016. Upscaling evapotranspiration measurements from multi-site to the satellite pixel scale over heterogeneous land surfaces. Agric. For. Meteorol. 230–231, 97–113.
Liu, S., Li, X., Xu, Z., Che, T., Xiao, Q., Ma, M., Liu, Q., Jin, R., Guo, J., Wang, L., Wang, W., Qi, Y., Li, H., Xu, T., Ran, Y., Hu, X., Shi, S., Zhu, Z., Tan, J., Zhang, Y., Ren, Z., 2018. The Heihe integrated observatory network: a basin-scale land surface processes observatory in China. Vadose Zone J. 17, 180072.
Martens, B., Miralles, D.G., Lievens, H., van der Schalie, R., de Jeu, R.A.M., Fernández-Prieto, D., Beck, H.E., Dorigo, W.A., Verhoest, N.E.C., 2017. GLEAM v3: satellite-based land evaporation and root-zone soil moisture. Geosci. Model Dev. 10, 1903–1925.
Merlin, O., Bitar, A.A., Rivalland, V., Béziat, P., Ceschia, E., Dedieu, G., 2011. An analytical model of evaporation efficiency for unsaturated soil surfaces with an arbitrary thickness. J. Appl. Meteorol. Climatol. 50, 457–471.
Norman, J.M., Kustas, W.P., Humes, K.S., 1995. Two source approach for estimating soil and vegetation energy fluxes in observations of directional radiometric surface temperature. Agric. For. Meteorol. 77, 263–293.
Priestley, C.H.B, Taylor, R.J., 1972. On the assessment of surface heat flux and evaporation using large-scale parameters. Mon. Weather Rev. 100 (2), 81–92.
Purdy, A.J., Fisher, J.B., Goulden, M.L., Colliander, A., Halverson, G., Tu, K., Famiglietti, J.S., 2018. SMAP soil moisture improves global evapotranspiration. Remote Sens. Environ. 219, 1–14.
Qiu, B., Chen, J.M., Ju, W., Zhang, Q., Zhang, Y., 2019. Simulating emission and scattering of solar-induced chlorophyll fluorescence at far-red band in global vegetation with different canopy structures. Remote Sens. Environ. 233, 111373.
Qiu, J., Crow, W.T., Dong, J., Nearing, G.S., 2020. Model representation of the coupling between evapotranspiration and soil water content at different depths. Hydrol. Earth Syst. Sci. 24, 581–594.
Song, L., Kustas, W.P., Liu, S., Colaizzi, P.D., Nieto, H., Xu, Z., Ma, Y., Li, M., Xu, T., Agam, N., Tolk, J.A., Evett, S.R., 2016. Applications of a thermal-based two-source energy balance model using Priestley-Taylor approach for surface temperature partitioning under advective conditions. J. Hydrol. 540, 574–587.
Song, L.S., Liu, S.M., William, P.K., Hector, N., Sun, L., Xu, Z.W., Todd, H.S., Yang, Y., Ma, M.G., Xu, T.R., Tang, X.G., Li, Q.P., 2018. Monitoring and validating spatially and temporally continuous daily evaporation and transpiration at river basin scale. Remote. Sens. Environ. 219, 72–88. https://doi.org/10.1016/j.rse.2018.10.002.
Stocker, B.D., Zscheischler, J., Keenan, T.F., Prentice, I.C., Seneviratne, S.I., Peñuelas, J., 2019. Drought impacts on terrestrial primary production underestimated by satellite monitoring. Nat. Geosci. 12, 264–270.
Twine, T.E., Kustas, W.P., Norman, J.M., Cook, D.R., Houser, P.R., Meyers, T.P., Prueger, J.H., Starks, P.J., Wesely, M.L., 2000. Correcting eddy-covariance flux underestimates over a grassland. Agric. For. Meteorol. 103, 279–300.
Wang, K., Dickinson, R.E., 2012. A review of global terrestrial evapotranspiration: observation, modeling, climatology, and climatic variability. Rev. Geophys. 50, RG2005.
Xu, Z., Liu, S., Li, X., Shi, S., Wang, J., Zhu, Z., Xu, T., Wang, W., Ma, M., 2013. Intercomparison of surface energy flux measurement systems used during the HiWATER-MUSOEXE. J. Geophys. Res.-Atmos. 118, 13140–113157.
Yao, Y., Liang, S., Yu, J., Zhao, S., Lin, Y., Jia, K., Zhang, X., Cheng, J., Xie, X., Sun, L., Wang, X., Zhang, L., 2017. Differences in estimating terrestrial water flux from three satellite-based Priestley-Taylor algorithms. Int. J. Appl. Earth Obs. Geoinf. 56, 1–12.
Zhang, K., Zhu, G., Ma, J., Yang, Y., Shang, S., Gu, C., 2019. Parameter analysis and estimates for the MODIS evapotranspiration algorithm and multiscale verification. Water Resour. Res. 55 (3), 2211–2231.
Zhou, S., Yu, B., Huang, Y., Wang, G., 2014. The effect of vapor pressure deficit on water use efficiency at the subdaily time scale. Geophys. Res. Lett. 41, 5005–5013.
Zhou, S., Yu, B., Zhang, Y., Huang, Y., Wang, G., 2016. Partitioning evapotranspiration based on the concept of underlying water use efficiency. Water Resour. Res. 52, 1160–1175.